Low-temperature ion-beam mixing in metals

S.-J. Kim and M-A. Nicolet
California Institute of Technology, Pasadena, California 91125

R. S. Averback
Argonne National Laboratory, Argonne, Illinois 60439
*and University of Illinois at Urbana-Champaign, Urbana, Illinois 61801**

D. Peak
Union College, Schenectady, New York 12308
(Received 7 November 1986)

A systematic study of ion-beam mixing of tracer impurities in thin metal films at low temperatures has been conducted. We have investigated the dependence of ion mixing on two matrix properties: atomic mass and cohesive energy. We have also studied the dependence of ion mixing on tracer impurity properties: its heat of mixing with the matrix and its thermal diffusivity in the matrix. The matrices investigated were thin films of C, Al, Ti, Fe, Ni, Cu, Mo, Ru, Ag, Hf, Ta, W, Pt, and Au. The tracer impurities, Al, Ti, Cr, Mn, Fe, Ni, Cu, Y, Nb, Mo, Ru, Ag, In, Sb, Hf, Ta, W, Pt, Au, and Bi, were deposited as ≤ 15 Å layers near the midplanes of the specimens. All the tracer and matrix elements, except C, were deposited sequentially, without breaking vacuum. The samples were irradiated with 300–1000-keV Kr ions to doses 10^{15}–10^{16} ions/cm^2 at temperatures of 6 and/or 77 K. Most samples were analyzed at the irradiation temperature by He backscattering. A strong correlation between ion mixing and the matrix properties, atomic mass, and cohesive energy, was observed. A correlation between ion mixing and tracer impurity diffusion was also observed but not between ion mixing and the heat of mixing or relative mass of the impurity with the matrix. The results are interpreted within the framework of a thermal spike model of cascade diffusion.

I. INTRODUCTION

Recent technological success in using ion beams for materials-modification applications has spurred a growing interest in the underlying science of the method. Ion-beam modifications can be achieved by various mechanisms.[1] Solute atoms can be implanted, thermal reactions can be accelerated, stable alloy phases can be induced to transform to metastable phases, and surface layers can be mixed with substrates. In all of these cases, success derives from the ability to overcome either thermodynamic or kinetic barriers by the use of energetic particles. An understanding of how these barriers are surmounted relies on the elucidation of the basic atomic displacement processes involved in particle irradiation and the relaxation of the highly nonequilibrium state following the displacement process. For example, it is known that many intermetallic compounds transform to an amorphous state under ion irradiation. Whether this transformation is caused by "rapid quenching" of a "molten" cascade zone, radiation-induced disorder, and/or the agglomeration of radiation-induced point defects, is still controversial. A fundamental knowledge of the displacement process in cascades would be very helpful in solving such problems. It has recently been shown that quantitative analysis of ion-beam-mixing experiments performed at low temperatures can help to ferret out basic displacement processes in energetic displacement cascades.[2,3]

In the last few years, several diffusion mechanisms have been espoused to explain ion-beam mixing (which we denote here as IM). Initially, IM was thought to be due to energetic collisional processes, i.e., collisional mixing.[4–7] Various theoretical models, both analytic[4–6] and computer simulation,[7] were derived on this premise. Inherent in all of these models are the assumptions that the relocation of target atoms requires collision energies >5 eV, the collisions are binary in nature, and the cascades are linear. It is not surprising that these models, as will be outlined below, have all proven inadequate. These same models had been employed to interpret a wide range of radiation-damage effects such as defect production and disordering of initially ordered alloys,[3] and they had been shown to be inadequate there also. In fact, it has been recognized for some time now that collective atomic motion during the thermal spike phase of the cascade must be incorporated into any realistic cascade model.[8,9]

The importance of thermal spikes for diffusion processes in cascades has recently been shown quite convincingly through a series of IM experiments. In one type of these experiments, IM was measured in a given target for different marker atoms.[10,11] Using markers either of similar or far different atomic mass as the matrix atoms, predictions based on solely kinematic models were proven inadequate. In another set of experiments,

it was demonstrated that IM in bilayer systems which had very similar physical properties but different chemical properties had very different IM characteristics. These latter experiments involved systems for which there was a large heat of mixing, either negative[12] or positive,[13,14] between atoms comprising the bilayer material. Johnson *et al.* pointed out that these chemical effects could be explained by applying a thermodynamic analysis of diffusion to IM.[2] Moreover, by noting that chemical interactions are of the order of tenths of an electron volt per atom, Johnson *et al.* deduced that the relevant energies of diffusion in cascades must similarly be tenths of an electron volt.[2] Thus, it is now recognized that thermal spike mixing is an important, if not dominant, contribution to IM at low temperatures.

Although the foundations for understanding IM and other ion-beam modification techniques are beginning to emerge, knowledge of the underlying mechanisms on an atomic scale is still rudimentary. One of the problems that has impeded progress has been the lack of a reliable set of IM data for many systems. Experimental work has been successful mostly at disproving theories and finding particular, but isolated, effects. There is now a need for sufficient experimental information to set guidelines for new theories. Therefore, this work was undertaken to establish a wide data base for IM in metal systems. To simplify comparison to theories, the experiments were carried out with few physical variables. First, nearly all irradiations were performed with the specimen approximately at liquid-helium temperature, and subsequent analysis, using backscattering spectrometry, was performed prior to warming. This procedure eliminates any possible thermally induced diffusion. In addition, the "marker geometry" was employed.[15,16] This geometry, which consists of a thin tracer impurity layer buried at some depth in the specimen, precludes many of the difficulties involved in extracting fundamental quantities from chemical diffusion coefficients which are often encountered when using bilayer samples.[17]

Our experiments comprise two interdependent parts. The first part investigates the influence of the elemental identity of the marker atoms in a given matrix on IM. The various markers were selected according to either their diffusivity in a specific matrix or by their heat of mixing with the matrix. To a lesser extent, the atomic mass of the marker relative to the matrix atoms was considered. The correlation between diffusivity and IM was investigated primarily using a Cu matrix since reliable diffusivity data for many tracer impurities in Cu are available. Other systems, however, were also employed. The relationship between the heat of mixing of the marker in a specific matrix was explored using several markers in both Mo and Ru. The second part investigates correlations between IM and the physical properties of the matrix element. The matrix properties of interest were the atomic mass and the cohesive energy. To obtain systematic results, the study required a large number of matrix elements and in each, at least two markers. To help provide the background for these experiments, a brief outline of the current theories of IM is presented. The experimental procedures are then described and the results given. We then compare the experimental results with theory to indicate the detail to which IM is presently understood.

II. THEORETICAL BACKGROUND

When an energetic particle impinges on a solid, it begins to slow down by making elastic nuclear collisions with host atoms and inelastic collisions with electrons. The latter collisions do not cause atomic displacements in metals, and, therefore, do not contribute to IM. The elastic collisions result in the displacement of target atoms from their initial lattice sites. The more energetic of these recoiling atoms can cause further displacements of host atoms; this process continues and results in a cascade of displaced atoms. The phase lasts $\approx 10^{-13}$ s; it is often designated as the collisional phase of a cascade. Several theoretical attempts have been made to calculate the contribution of this collisional mixing process to IM. These include both analytical transport theory[5,6] and computer simulation.[7] The underlying assumptions in collisional mixing calculations are (a) the collisions are governed by two-body interactions; (b) moving atoms collide only with stationary atoms, i.e., linear cascades; (c) the targets are amorphous; and (d) the displacement process ends when the atom energies fall below ≈ 5 eV. The principal results of these calculations are the following:

(1) The spreading of a marker layer has a Gaussian distribution.

(2) The variance, σ^2, of the distribution increases proportionally to the ion fluence, Φ, and to the damage energy-deposition rate per ion, F_D (i.e., F_D is the damage energy dE_D per depth dx and per ion which goes into elastic nuclear collisions. The damage energy E_D excludes the energy deposited in electronic excitations).

(3) The magnitude of IM can be obtained approximately from,[6]

$$\sigma^2=(1/3\Gamma_0)(1/N)(\Phi F_D)\gamma_{21}\langle r^2\rangle/E_d \ . \tag{1}$$

$\Gamma_0=0.608$, N is the atomic density of the matrix, r is the distance a target atom is displaced when recoiling, E_d is the average energy per displaced atom, and

$$\gamma_{21}=\sqrt{4(m_1m_2)/(m_1+m_2)^2} \ . \tag{2}$$

Although it now seems that the contribution to IM from collisional displacements is not as large as other contributions, this theory still provides a useful method to compare IM data from different targets under different irradiation conditions. For a marker experiment, an effective diffusion coefficient for IM, D, can be extracted from measurements of σ^2 from the expression

$$Dt=\sigma^2/2 \ , \tag{3}$$

where t is the time of the irradiation. We define the normalized quantity,

$$\xi=Dt/\Phi F_D \ , \tag{4}$$

and denote it as the mixing efficiency. From Eqs. (1) and

(3) it can be seen that ξ is independent of the irradiation particle and dose. Moreover, as $\langle r^2 \rangle / E_d$ is not expected to vary greatly from target to target, the mixing efficiency should not be sensitive to the target. Thus, by comparing IM data on the basis of mixing efficiency, the influence of various parameters on IM can be systematically investigated. This procedure has been found very useful for basic investigations of other radiation effects.[3]

At the end of the collision phase of the cascade, there is a residual agitation of the atoms in the cascade region. This condition is often referred to as a thermal spike; it lasts $\approx 10^{-11}$ s. This residual agitation stimulates atomic diffusion; we will denote this process as thermal spike diffusion. Different models for thermal spike diffusion have been developed. A particularly instructive model is due to Vineyard.[18] This model assumes that the initial energy distribution has the form of a linear δ function, to represent the track of the ion, and that the temperature distribution evolves in time according to classical heat-flow theory. The model further assumes that a thermally activated diffusional jumping process occurs in the region of the spike with a jump rate

$$\eta = A \exp(-Q/\tau) , \tag{5}$$

where τ is the product of Boltzmann's constant and temperature. The total number of jumps in the cascade calculated under these conditions is

$$\eta = A \lambda^2 / 8\pi\kappa C Q^2 , \tag{6}$$

where λ is the energy per unit length along the track of the ion, κ is the thermal conductivity for lattice heat conduction, and C is the specific heat of the target. The Vineyard model provides a phenomenological model of diffusion in cascades; it does not deal with the mechanisms of diffusion. Johnson *et al.*[2] have suggested that the activation enthalpy for the jumping process, the parameter Q in Eqs. (5) and (6), is related to the cohesive energy of the target.[2] Van Rossum *et al.* have in fact shown that, for bilayer samples, IM does correlate with the cohesive energy.[19]

Molecular-dynamics computer simulations provide a far more detailed picture of the dynamics of cascade processes which includes both the production of Frenkel pairs (i.e., vacancies and interstitial atoms) and the excitation of the lattice.[9,20] These simulations indicate that point defects are produced during the collisional phase of the cascade and that they subsequently undergo stimulated motion, which is responsible for thermal spike diffusion, during the thermal spike phase of the cascade. Unfortunately, these simulations have been performed for cascade energies of only a few kiloelectron-volts, and mostly for potentials describing W. It is uncertain at this time whether diffusion in higher energy cascades, or in cascades in less refractory metals, involves yet other diffusion mechanisms. Nevertheless, a simple point-defect model for thermal spike diffusion has been developed[21] based on the results of these simulations. The model assumes that diffusion in cascades consists of normal radiation-enhanced diffusion, but it is limited to very short times, $\approx 10^{-11}$ s, and to very high temperatures. The effective diffusion coefficient during the spike is given by

$$D(t) = D_i c_i D_v c_v , \tag{7}$$

where c_i and c_v are the instantaneous interstitial atom and vacancy concentrations within the spike, respectively, and

$$D_i = D_{0i} \exp(-\Delta H_{1i}^m / \tau) , \tag{8a}$$

$$D_v = D_{0v} \exp(-\Delta H_{1v}^m / \tau) . \tag{8b}$$

ΔH_{1i}^m and ΔH_{1v}^m are the enthalpies of migration for single interstitial atoms and monovacancies, respectively. The initial conditions of the cascade can be obtained using parameters from binary collision calculations as the initial conditions are not influenced by thermal spike effects.[9] The initial point defect concentration is obtained using the Kinchin-Pease expression[22] for the number of point defects produced in a cascade; the tables of Winterbon[23] are used to obtain the volume of the cascade at the end of the collision phase, $V_d(t=0)$. The initial temperature of the cascade is deduced from the expression

$$3\tau = E_D / [N V_d(t=0)] . \tag{9}$$

E_D is the damage energy in the cascade; it too is obtained using the Winterbon tables.[23] The evolution of the temperature and point-defect distributions are calculated by standard heat-flow and reaction-rate equations. The spreading of a thin marker is calculated within this model using[21]

$$\langle \Delta x^2 \rangle = 2\Phi \int dT (d\sigma'/dT) \int N V_d(t) D(t) dt , \tag{10}$$

where $d\sigma'/dT$ is the cross section for producing a recoil of energy T, and $V_d(t)$ and $D(t)$ are the time-dependent volumes and diffusion coefficients for cascades of energy T. The approximations employed to solve Eq. (10) can be found in Ref. 21. Although this spike model retains the spirit of the Vineyard model, it specifies a diffusion mechanism, and semiquantitative calculations can be performed. The physical parameters such as the energy density in the spike and the cohesive energy are contained implicitly in this model through the diffusion coefficient and point-defect concentrations. The energy density determines the temperature of the spike. The cohesive energy is related to the point-defect mobilities and to the concentration of point defects produced in the spike. One of the goals of the present experiments is to test the predictions of this model by varying the target and marker species so as to affect the migration enthalpies, point-defect concentrations, and spike temperature.

III. EXPERIMENTAL PROCEDURE

The marker samples were prepared by vapor deposition onto Si wafers which contained thick (≈ 1 μm) SiO_2 surface layers. The inert SiO_2 layers prevented interaction between the Si and the samples during irradiation. The substrates were cleaned organically and immediately loaded into an electron-gun evaporation system. The pressure was less than $\approx 10^{-7}$ Torr during evaporation.

The complete set of experiments included the matrix elements C, Al, Ti, Fe, Ni, Cu, Mo, Ru, Ag, Hf, Ta, W, Pt, and Au, and marker elements Al, Ti, Cr, Fe, Mn, Ni, Cu, Y, Nb, Mo, Ru, Ag, In, Sb, Hf, Ta, W, Pt, Au, and Bi. The thicknesses of the marker layers were $\approx 5-15$ Å, and these layers were located at the midplanes of the specimens which were $\approx$ 800 Å total thickness. All of the matrix and marker elements, excepting C, were evaporated sequentially using e^- beam heating in the same vacuum system without breaking vacuum. Carbon samples were prepared in another chamber by rf sputtering. A carbon layer was deposited first, followed by the deposition of the marker layer, and finally covered by the top matrix layer. A layer of Si, ≈ 30 Å thick, was deposited on the tops of most samples to minimize reactions with air after removing the samples from the vacuum system. It is commonly believed that oxygen contamination can inhibit IM in marker specimens. Some of the Mo specimens contained a small amount of W, much less than 1 at. %. This W contamination resulted from using a W crucible for the Mo charge in the e^--beam evaporator. Since W is totally soluble in Mo (Ref. 24) and the content of W was very small, we do not expect the IM results to be affected by the contamination. Comparison of results from two Mo samples containing Pt marker layers, one with and one without W contamination, showed no significant difference in IM.

For the *in situ* low-temperature experiments, the samples were irradiated and subsequently analyzed while clamped to the cold finger of a cryostat which was held at ≈ 6 K. A platinum-resistance thermometer was attached to the cold finger. The vacuum system and beamline were pumped with ion and cryopumps. The pressure in the target chamber during irradiation was $\approx 10^{-8}$ Torr. Kr ions, in the range 500 and 1000 keV, were employed for the irradiations. The specific energy for each matrix was selected so that the projected range of the Kr ions was approximately 3 times the initial marker-layer depth. This condition yields damage distributions that are similar for all irradiations and that are not rapidly varying at the marker position. The beam power on the specimen was maintained below 0.1 W to avoid heating. During the irradiation, the specimen normal was aligned 10° from the beam axis. The fluence was measured by integrating ion current collected on an annular disk that intercepted a portion of the beam. The calibration of the disk was checked with a moveable Faraday cup prior to and after each irradiation. The accuracy is about 5%.

The amount of IM was measured by backscattering spectroscopy (BS) using 1.9-MeV He ions from the same accelerator as was used for the Kr irradiations. The resolution of the detector system for the BS analysis was ≈ 15 keV. The scattering angle was $\approx 135°$, with the detector in the horizontal plane through the beam axis. The angle between the He beam and the sample normal was varied from $-5°$ (i.e., toward the detector) to $+35°$ about the vertical axis to maximize the resolution while maintaining sufficient separation of the matrix and marker signals.

For most of the measurements on the Mo and Ru matrices, different irradiation and BS systems were employed. The conditions of the experiments were also somewhat different; the Kr ion energy was 300 keV and the irradiations were performed at 77 K, not at 6 K. Moreover, these samples were warmed to room temperature and transferred to a separate system for BS analysis with 2-MeV He. To verify that there was no significant difference between the two procedures, samples of Ru with a Au marker and of Mo with Ti and Pt markers were irradiated and measured both ways. For Ru, the two results were within experimental uncertainty; for Mo, IM was slightly higher at 77 K than at 6 K, but it was not sufficiently different to interfere with the purpose of the experiment. These results are listed in Tables I and II. In the experiment investigating the correlation between impurity diffusion coefficients and IM efficiency in a Cu matrix, the samples were irradiated with 750-keV Kr at 77 K and were BS analyzed *in situ* using 1.9-MeV He. The samples with Pt or Au markers were also irradiated at 6 K, and their IM efficiencies were within experimental uncertainty to those irradiated at 77 K. These results are tabulated in Table III.

All backscattering signals from the marker elements had Gaussian distributions both before and after the irradiations. The increases in the variances of the marker distributions due to IM were calculated from

$$\Omega^2 = \Omega^2_{\text{irr}} - \Omega^2_{\text{unirr}} , \tag{11}$$

where Ω^2_{irr} and Ω^2_{unirr} are the measured variances of the marker signals from the irradiated and unirradiated samples, respectively. The standard deviation for the broadening of the marker profile, σ, in units of length, was calculated with

$$\sigma = \Omega / N[\varepsilon] , \tag{12}$$

where N and $[\varepsilon]$ are the atomic number density and the stopping-cross-section factor of the matrix, respectively. The effective diffusion coefficient for IM was then obtained by use of Eq. (3).

IV. RESULTS

Typical backscattering spectra acquired before and after Kr irradiation at 6 K are shown in Fig. 1. The spectra here represent a Ag marker in Cu. The values of Dt derived from these data were found to be linearly proportional to the ion fluence, Φ. A linear relationship between Dt and Φ is a common feature for IM in metal marker systems at low temperatures.[25] We have used this relationship between Dt and Φ as a criterion for the validity of our data; hence, all samples were irradiated to two or more fluences. A linear increase of Dt with fluence was found in nearly all cases. In our initial specimens of Al with a Pt marker, Fe with Pt, Fe with Au, and Ni with Pt, a nonlinear dose dependence was observed. These experiments were repeated with a new batch of samples, and for these, a linear dose dependence of Dt was observed. The cause of the spurious results for the initial samples is unknown, although we suspect contaminations (despite our efforts to minimize them). This result is indicative of the difficulty of obtaining reli-

TABLE I. Ion-mixing data for different matrix materials. Irradiation conditions and symbols in table are given in text.

Matrix	Marker	E_{irr} (keV)	F_D (eV)	$Dt/\phi F_D$ (Å^5/eV)	$T_{1/2}$ (keV)	E_r (keV)	V_t (Å^3)	ΔH_{coh} (eV/atom)	δ (kJ/mol)
C	Ni	500	81.2	2.60	10	5.6	883 401 655	7.36	
C	Ag	500	81.2	2.30	10	5.6	883 401 655	7.36	
C	Au	500	81.2	2.70	10	5.6	883 401 655	7.36	
Al	Ag	650	58.4	20.70	28	17.1	11 494 920	3.33	−22
Al	W	650	58.4	22.50	28	17.1	11 494 920	3.33	−8
Al	Pt	650	58.4	12.70	28	17.1	11 494 920	3.33	−185
Ti	Mo	500	107.4	4.50	50	32.1	7 436 669	4.87	−16
Ti	Hf[a]	300	118.7	11.00	50	32.1	7 436 669	4.87	+1
Ti	Pt[a]	300	118.7	3.30	50	32.1	7 436 669	4.87	−337
Fe	Pt	650	117.0	4.50	65	41.8	2 179 690	4.31	−59
Fe	Au	650	117.0	4.60	65	41.8	2 179 690	4.31	+38
Ni	Pt	650	210.0	5.00	65	42.0	1 434 996	4.44	−22
Ni	Au	650	210.0	7.80	65	42.0	1 434 996	4.44	+34
Cu	Pt	650	189.0	23.20	65	42.6	1 035 344	3.50	−32
Cu	Au	650	189.0	27.40	65	42.6	1 035 344	3.50	−29
Mo	Al	500	197.0	5.80	80	54.6	1 668 422	6.81	−20
Mo	Ti	500	135.0	1.65	80	54.6	1 668 422	6.81	−16
Mo	Pt	650	198.0	6.00	80	54.6	1 668 422	6.81	−115
Ru	Au	500	236.0	7.40	82	56.3	1 018 853	6.74	+65
Ag	Al	650	197.0	93.4	85	58.6	1 751 618	2.96	−21
Ag	Pt	650	197.0	59.0	85	58.6	1 751 618	2.96	−1
Hf	Ti	750	207.0	12.7	110	82.0	2 112 571	6.44	+1
Hf	Ni	750	207.0	17.2	115	82.0	2 112 571	6.44	−147
Ta	Fe	1000	207.0	7.6	115	82.1	1 151 776	8.10	−54
Ta	Ni	1000	207.0	10.4	115	82.1	1 151 776	8.10	−104
Ta	Y	1000	207.0	3.5	115	82.1	1 151 776	8.10	+127
W	Fe	1000	243.0	7.5	115	82.2	719 143	8.66	0
W	Ni	1000	243.0	17.9	115	82.2	719 143	8.66	−11
W	Y	1000	243.0	2.2	115	82.2	719 143	8.66	+110
Pt	Fe	1000	271.5	23.9	110	79.0	479 170	5.85	−47
Pt	Ni	1000	271.5	14.2	110	79.0	479 170	5.85	−17
Au	Ni	1000	271.5	58.0	110	79.4	654 839	3.80	+25
Au	Cu	1000	271.5	142.0	110	79.4	654 839	3.80	−20
Au	Cu	1000	271.5	165.0	110	79.4	654 839	3.80	−20

[a]These samples were irradiated at 77 K and analyzed at 300 K.

TABLE II. Dependence of IM efficiency on heat of mixing parameter, δ, for several markers in Mo and Ru matrices.

Matrix	Marker	$Dt/\Phi F_D$ (Å^5/eV)	δ (kJ/mol)
Mo	Ti	7.6	−16
Mo	Cr	7.6	+1
Mo	Ni	10.3	−27
Mo	Hf	3.7	−15
Mo	Ta	5.0	−20
Mo	Pt	8.5	−115
Mo	Au	13.4	+15
Ru	Ti	8.9	−191
Ru	Cr	14.7	−42
Ru	Mn	10.7	−40
Ru	Ni	5.8	+2
Ru	Hf	3.7	−227
Ru	Ta	6.6	−164
Ru	Pt	2.0	−4
Ru	Au	6.4	+65

able data with markers. In assessing the uncertainties in our results, we believe that the greatest errors arise, in fact, from specimen contamination rather than from inaccurate measurements. The latter we estimate to be less than $\approx 15\%$. For the more noble metals, the reproducibility of results was of this order. For the refractory

TABLE III. IM efficiencies, impurity diffusion coefficients, and heat-of-mixing parameters for several markers in Cu.

Markers	$Dt/\Phi F_D$ (Å^5/eV)	D_{imp} (Å^2/s)	δ (kJ/mol)
Nb	24.6	4.2×10^6	−10
Ru	15.3	1.0×10^7	+49
Ag	38.2	1.6×10^8	+5
In	47.3	5.0×10^8	+1
Sb	43.5	5.8×10^8	−12
Pt	25.0	4.3×10^6	−32
Au	27.0	5.9×10^7	−29
Bi	36.5	1.1×10^9	+27

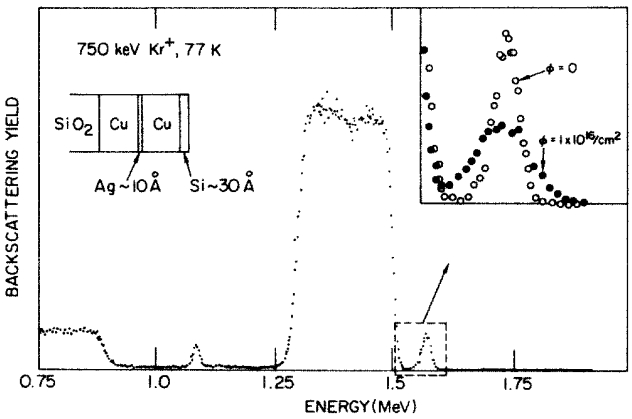

FIG. 1. Typical backscattering spectra showing the spreading of a thin marker during ion irradiation. Here, the spectra illustrate Ag spreading in a Cu matrix for 500-keV Kr irradiation at 6 K for three doses.

metals, for which the mixing efficiency was small and high fluences were necessary, the uncertainties can probably be best estimated as 15% ± 3 Å^5/eV. We cannot be confident that differences in mixing efficiencies less than ≈ 3 Å^5/eV are meaningful unless the experiments were repeated with different samples.

Comparison of the data from different samples and irradiation energies requires a normalization procedure. As indicated above, normalizing the data by the damage energy per unit volume is a natural method for radiation effects. (This is sometimes expressed in the equivalent units of displacements per atom.) To determine the damage energy at the marker depth for the various irradiations, the computer-simulation program, TRIM, was employed.[26] Figure 2 illustrates damage energy distributions for three irradiations employed in this study. Note

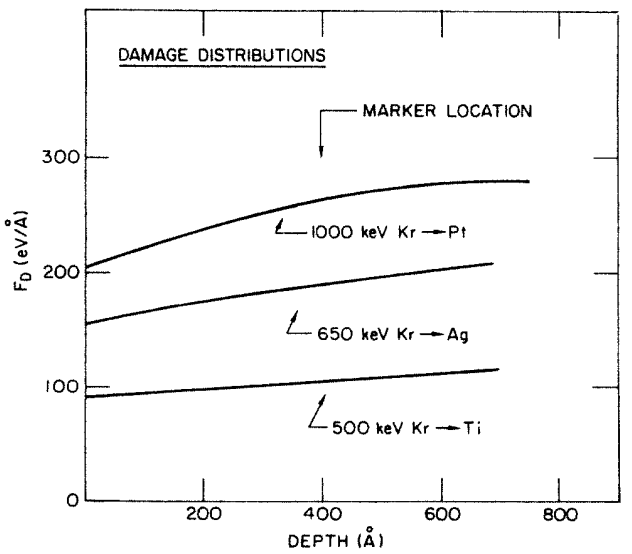

FIG. 2. Damage energy distributions for three representative projectile-target combinations. Calculations were performed using TRIM (Ref. 26).

that at the initial marker depth the deposited damage energy, F_D, does not change rapidly with depth. The average value of F_D within a 200-Å region centered at the initial marker depth was employed for normalization. The complete set of data for these marker experiments is tabulated in Tables I–III. The normalized data are the values of the mixing efficiency $\xi = Dt/\Phi F_D$.

Table I illustrates that the mixing efficiency varies significantly from matrix to matrix. Moreover, within a given matrix, the mixing efficiency also varies from marker to marker. This second result is contrary to the early expectation that IM would be independent of the chemical nature of the tracer impurity. The influence of the type of marker on IM has been noted previously for the semiconductor matrices, Si (Ref. 10) and Ge (Ref. 11) and for the metallic matrix, Hf (Ref. 27). These studies, however, were limited to a few markers. Only in Al has IM been measured at low temperatures for a large number of markers, and for it, no significant variation was observed.[28] In the present study, we have investigated correlations between three marker properties and IM: the impurity diffusion coefficient of the marker in the matrix, the heat of mixing between marker and matrix, and the relative atomic mass of the marker and matrix atoms.

In attempting to correlate the low-temperature mixing efficiencies with impurity diffusion parameters, an ambiguity arises since impurity diffusion is temperature dependent, i.e.,

$$D_{\text{imp}} = D_0 \exp(-Q/\tau) \, . \tag{13}$$

D_{imp} is the impurity tracer diffusivity, D_0 is a prefactor, and Q is the activation enthalpy for diffusion. For diffusion of substitutional solutes in metals, Q is the sum of the enthalpies of vacancy migration and vacancy formation. Thus, to correlate mixing efficiency with impurity diffusivities, a "comparison temperature" must be selected. An alternative is to correlate IM with D_0 or Q, separately. For the present, we correlate the mixing efficiency with impurity diffusivity (obtained by extrapolation) at the melting temperature of the matrix. At this temperature, D_{imp} is far more sensitive to changes in Q than D_0 so that this correlation is effectively also a correlation between IM and Q. We have selected Cu as the matrix element for this comparison, as reliable diffusion data are available for many tracer impurities in Cu. The results are plotted in Fig. 3 (Note the logarithmic scale). A clear correlation between D_{imp} and the mixing efficiency, $Dt/\Phi F_D$, is evident. Similar correlations, although based on many fewer data, seem to exist for Ag and Au matrices. These matrices, like Cu, are good thermal spike metals. The relevant data are in Tables I and III.

The influence of the heat of mixing between the marker and matrix on IM was also investigated. It should be pointed out that within both collisional and thermal spike diffusion models of IM, such an influence should be small. Nevertheless, such a correlation has been reported;[29] moreover, our first measurements of IM in various hosts seemed to depend on the heat of mixing,

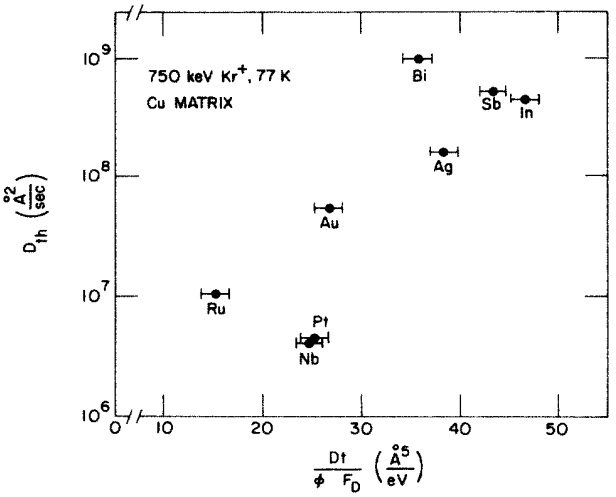

FIG. 3. Plot illustrating the correlation between the tracer diffusion coefficients of various impurities in Cu, at the melting temperature, with the mixing efficiency of these impurities at low temperature.

ΔH_m (note values of the mixing efficiency for Ag, Ta, W, Pt, and Au matrices). Therefore, an experiment was carried out to determine the importance of the heat of mixing in the mixing efficiency of a marker. Mo and Ru were selected as matrices for this study as they have very similar physical properties, but different markers have far different values of the heat of mixing with each. The influence of ΔH_m in Cu was also considered. The results of these studies are tabulated in Tables II and III; they are graphically shown in Fig. 4; here, the mixing efficiency, ξ, is plotted as a function of the heat of mixing parameter, δ (i.e., $\Delta H_m = 2\delta C_A C_B$). This parameter is the nearest-neighbor bond-energy difference of Miedema[30] and C_A and C_B are the local concentrations of atoms A and B. Although there are variations in ξ for the different markers in each matrix, and the same markers in the two matrices, as large as a factor of ≈ 5, there is no obvious trend between the mixing efficiency and the heat of mixing.

The same data obtained here for the investigations of the correlations between both the heat of mixing and impurity diffusivity with IM can also be employed to check for possible correlations between the relative atomic masses of the marker and matrix and the mixing efficiency. Figure 5 shows values of $Dt/\Phi F_D$ in Mo, Ru, and Cu for various marker elements plotted in sequence of increasing atomic mass of the marker. There is no systematic dependence of mixing efficiency on the atomic mass of the marker. Variations of the mixing efficiency with the atomic mass of the marker are therefore small in comparison to its variation with other factors. In summary, this set of experiments illustrates that IM depends on the type of marker in a given matrix. Variations in the mixing efficiency are typically less than a factor of $\approx 2-3$ for a given matrix, although between extrema they can be larger. The mixing efficiency in Cu at 77 K correlates with tracer impurity diffusion coefficients. It does not, on the other hand, depend on the heat of mixing or the relative atomic mass of the marker with the matrix at 77 K.

The second part of these experiments investigates the role of the physical properties of the matrix in ion mixing. As the first part of our study has shown that IM in a given matrix depends on the type of marker, by virtue of the diffusivity of that marker (and perhaps other unknown factors), a basis for comparing IM for different matrices is required. A common method in diffusion studies is to compare only self-diffusion data. The use of tracer isotopes for IM studies is impractical as the current understanding of IM does not warrant such detailed information. Tracer isotopes have been used in one study of IM, Cu,[14] and it was found that the results were not far different from suitably chosen marker impurities. Another approach, and the one employed here, is to measure IM for several markers in a given matrix and to define an average mixing efficiency for the matrix from these measurements. Thus, the mixing efficiency for each matrix in this study represents an average from at least two markers. Two markers, of course, do not guarantee that the "average" value of ξ for the matrix is

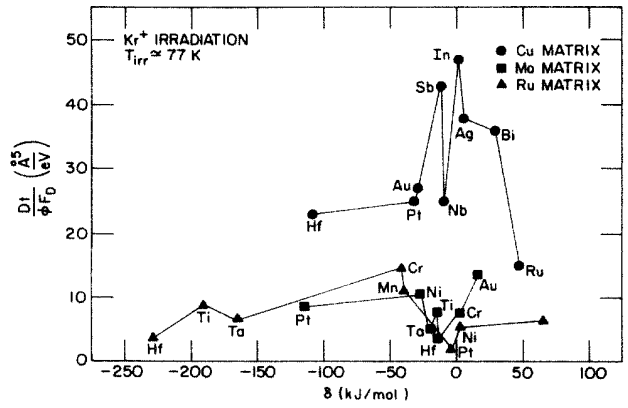

FIG. 4. Plot of the mixing efficiency as a function of the heat of mixing parameter, δ, between various marker elements with Cu, Mo, and Ru matrices.

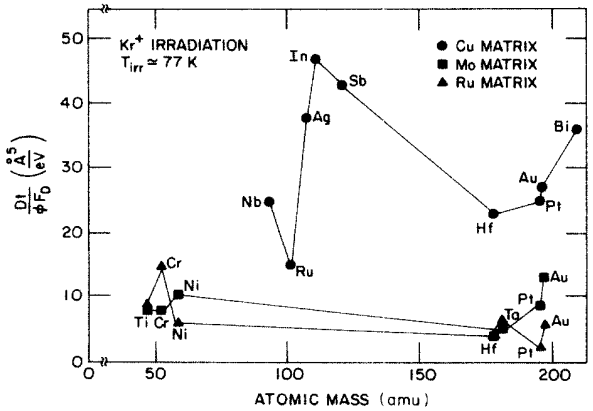

FIG. 5. Plot of the mixing efficiency as a function of the atomic mass of the marker for various markers in Cu, Mo, and Ru matrices.

obtained, but it does prevent one particularly unusual value of ξ from playing too dominant a role in this study.

The results for the average mixing efficiencies in the various matrices are plotted in Fig. 6. The figure was constructed to explicitly illustrate the influence on IM of the two physical properties of the target suggested by Eq. (6), energy density in the cascades and cohesive energy. The ordinate in this plot is a measure of the square of the energy density in the cascades [λ^2 in Eq. (6)], and the abscissa is a measure of the square of the inverse cohesive energy [the cohesive energy is related to Q in Eq. (6)]. The circles in the plot are located according to the energy density and cohesive energy of the matrix (indicated by the symbol in the circle). The value of the mixing efficiency for the target is contained in the circle; it is the average of our results for all the different markers in that matrix obtained at 6 K. The qualitative features of the influence of the properties of the matrix on IM are apparent in the figure. For a given value of the cohesive energy of the target, the mixing efficiency increases with increasing energy density (vertical translations in the plot); for a given value of the energy density, the mixing efficiency increases with increasing values of the inverse cohesive energy (horizontal translations).

Two choices were possible to represent the energy density in the plot, the linear energy density along the path of the projectile, or the volume energy density associated with a spike. For the relatively-high-energy ions employed in this study, the second choice was preferred. High energy ions have a long mean free path between high-energy collisions and produce several isolated subcascades along their tracks.[31,32] This process is not well described by a smooth deposition of energy along the projectile track. The energy density for each target was therefore obtained from the damage energy within "typical" subcascades, E_v, and the volume of these subcascades, V_t. The energy in the typical subcascade, $T_{1/2}$, was determined from Eq. (8),

$$0.5=(1/E_D)\int_0^{T_{1/2}} dT\,[d\sigma'(E,T)/dT]E_D(T)\ , \quad (14)$$

where $E_D(T)$ is the damage energy associated with a recoil of energy T, and E_D is the total damage energy. Half of the damage energy, therefore, is deposited in subcascades with recoil energies greater than $T_{1/2}$, and half the damage energy is deposited in recoils below $T_{1/2}$. In this way, $T_{1/2}$ is the typical recoil energy. The volumes of the subcascades are determined from[33]

$$V_t=\tfrac{4}{3}\pi[\beta(\langle\Delta x\rangle^2+2\langle y\rangle^2)]^{3/2}\ , \quad (15)$$

where Δx and y are the longitudinal and transverse straggling, respectively, and β is a contraction factor relating individual cascades to distribution averages. Values for the straggling were obtained from Winterbon's tables.[23]

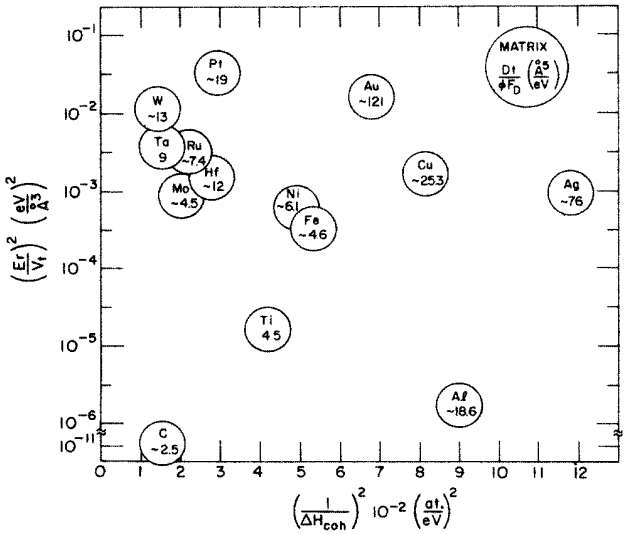

FIG. 6. Plot of the mixing efficiency as a function of the square of the energy density, the ordinate, and as a function of inverse square of the cohesive energy, the abscissa. The matrix element and the efficiency are identified in the circle.

V. DISCUSSION

The results of these experiments can be briefly summarized as follows.

IM depends on the physical properties of the target. Values of the mixing efficiency increase as the energy densities in the cascades increase and as the cohesive energies of the matrices decrease. These effects are pronounced; the mixing efficiency varies from ≈ 5 Å^5/eV for Ti to ≈ 100 Å^5/eV for Au. IM also depends on the type of marker in the matrix. In Cu, the mixing efficiency scales with the tracer impurity diffusion coefficient of the marker. The variation of the mixing efficiency with the type of marker within a matrix is less pronounced than its variation with the type of matrix. In most matrices, the variation is less than a factor of $\approx 2-3$. No apparent correlation exists between IM and the heat of mixing or the relative atomic masses of the marker and matrix.

The absence of a significant influence of the heat of mixing (Fig. 4) on the mixing efficiency observed here for our marker experiments contrasts with the strong effect the heat of mixing has in bilayers.[2] We interpret this result as a confirmation that the experimental technique of placing a thin impurity layer in a matrix adequately approximates the conditions necessary for a tracer impurity diffusion measurement. This conclusion is further supported by the linear dose dependence of the variances of the impurity distributions. In this regard, transmission-electron-microscopy studies of the immiscible marker systems would be very helpful in determining whether precipitation is present.

The sum of our results finds no reasonable interpretation within collisional models of IM. First, we note the magnitude of the mixing efficiency values. Collisional models predict values on the order of 1–5 Å^5/eV; these are much smaller than most of the experimental values. Second, the collisional theory of IM does not predict a strong dependence of the mixing efficiency on either the matrix or the type of marker. The target-sensitive parameter, $\langle r^2\rangle/E_d$, should not vary by an order of mag-

nitude in different targets. Moreover, it is expected that $\langle r^2 \rangle / E_d$, if anything, should decrease with increasing atomic mass of the matrix since the range of an atom of energy E_d would be smaller in the higher-atomic-mass materials. This prediction is just the opposite of our experimental results. Finally, the correlation of IM with tracer impurity diffusion coefficients is also at variance with the collisional model. The diffusivities of different tracer impurities vary, presumably due to small differences in their activation enthalpies for diffusion, usually some tenths of an electron-volt. Since E_d is greater than 5–10 eV,[5–7] such small differences cannot have any significant influence in collisional models. Thus, these experiments suggest that the contribution of collisional mixing, in most cases, is a secondary contribution. This conclusion is not new; however, it is established here systematically and as a general conclusion for IM in metals.

The correlations of IM with various matrix and marker properties support the hypothesis of thermal spike diffusion in cascades. The results agree qualitatively with the model calculations of Vineyard. Figure 6 illustrates that the mixing efficiency increases as the energy density in the cascades increases, in accordance with Eq. (6). Moreover, if we relate the activation enthalpy Q to the cohesive energy of the target, as suggested by Johnson *et al.*,[2] we find a dependence of the mixing efficiency on the cohesive energy, which is also predicted by Eq. (6). The lack of any dependence of IM on either the relative atomic masses and the heat of mixing for the marker and matrix also fit within the framework of thermal spike diffusion. The Vineyard model for thermal spike diffusion, however, does not enable one to calculate the absolute magnitude of the mixing efficiency since the model is mathematical and not physical; no diffusion process is specified in the model. For the same reason, the correlation between the mixing efficiency and the impurity diffusivity of the marker is not explicitly included in the Vineyard model [see Eq. (6)]. Presumably, the chemical properties of markers influence the activation enthalpies, Q. The lowering of the activation enthalpy for diffusion is believed to be a result of an electrostatic interaction between the impurity and a vacancy.[34,35] If the correlation between impurity diffusivity and thermal spike diffusion, noted here for Cu, is more than fortuitous, an explanation based on point-defect diffusion in a spike should be considered.

Radiation-enhanced diffusion theory, applied to the microscopic dimensions and time scale of a cascade, provides a natural interpretation for our results. The energy density in the cascades is important, as it determines the spike temperature, Eq. (9). The cohesive energy of the target is reflected through both the migration enthalpies and concentrations of the point defects in the spikes. The former is derived from the Van Liemp or other similar relations,[36] and the latter from the Kinchin-Pease expression, noting that the displacement energy tends to correlate with cohesive energy. The correlation of mixing efficiency with impurity diffusivity data also follows directly. The interaction between the impurity and vacancy lowers the activation enthalpy for diffusion. This reduced activation enthalpy is manifested in IM through a lowering of the vacancy migration enthalpy. The primary question to be addressed is whether the model adequately accounts for the magnitude of the mixing efficiency.

Before discussing the calculations of the mixing efficiency, we note that the migration enthalpies of self-interstitial atoms are much lower than vacancies.[37] The results of mixing experiments suggest, however, that the vacancy is responsible for thermal spike diffusion. This conclusion is deduced from the fact that thermal diffusion of substitutional impurities in metals is governed by a vacancy process;[38] consequently, a correlation between thermal diffusion and IM should, presumably, involve vacancies. Another result pointing to vacancy diffusion is the correlation of IM with cohesive energy. The migration enthalpy of vacancies tends to scale with cohesive energy of the matrix; for self-interstitial atoms this does not seem to be the case.[37] Thus, the interpretation of the experimental results within the radiation-enhanced diffusion model seems more reasonable assuming that vacancy motion, and not interstitial motion, is the predominant mechanism of thermal spike diffusion. A physical argument supporting this possibility derives from the structure of cascades. It is believed that during the collision phase of the cascade evolution many atoms are ejected from the core region, creating a "depleted zone." Thus vacancies are located in the hot-core region of the spike and interstitials in the cooler periphery region. Moreover, it has been found—using molecular-dynamics simulations—that in a region of high vacancy concentration, the vacancy migration enthalpy is reduced.[39] The molecular-dynamics simulations of cascades in W, to which we referred previously, have shown that in small cascades vacancies cause nearly as many atomic replacements as self-interstitial atoms and that their apparent migration enthalpy is much reduced from that deduced from equilibrium measurements.[9]

Based on the above considerations, values of the mixing efficiency have been calculated using Eq. (10) under the assumptions that vacancy migration enthalpies are reduced to one third of their "normal" values and that interstitial atoms are immobile.[40] Values for D_{0v} and ΔH_{1v}^m were deduced from a compilation of tracer impurity diffusion data in metals.[41] The results of these calculations are listed in Table IV. Experimental and calculated values of the mixing efficiency agree remarkably well. The calculated values agree within a factor of ≈ 2 of the experimental values, and they show the correct dependencies on cohesive energy and energy density. Part of the significance of this calculation is that it demonstrates that thermal spike diffusion can be understood, at least semiquantitatively, within the framework of our current understanding of radiation-damage theory. It does require, however, rather low values for vacancy migration enthalpies.

A second calculation was performed using this model to examine the correlation between mixing efficiency and impurity diffusion in Cu. Table V lists the results of the calculations for three possible values of the vacancy mi-

TABLE IV. Calculated values of the mixing efficiency using the radiation-enhanced diffusion model for thermal spike diffusion.

Host	ΔH_{1v}^m (eV)	D_{v0} (Å^2 s^{-1})	$\langle \Delta x^2 \rangle / 2\Phi F_D$ (Å^5 eV^{-1}) Predicted	Measured
Ag	0.65	1.6×10^{15}	56	60–90
Al	0.61	8×10^{14}	24	20–40
Au	0.82	1.4×10^{14}	70	80–140
Cu	0.69	6×10^{14}	19	20–26
Fe	1.17	3×10^{14}	3	6–7
Mo	1.30	2×10^{15}	16	6
Ni	1.39	8×10^{14}	6	8–10
Pt	1.39	1×10^{14}	24	16–24
W	1.69	7×10^{13}	11	6–15

gration enthalpy, ΔH_{1v}^m, $\frac{2}{3}\Delta H_{1v}^m$, and $\frac{1}{2}\Delta H_{1v}^m$. Values for ΔH_{1v}^m were deduced from Ref. 41. The magnitude of mixing efficiency agrees best for the lowest migration enthalpy, and the relative mixing efficiencies agree best for the highest migration enthalpy. The value of $\frac{2}{3}\Delta H_{1v}^m$ is a reasonable compromise. The reason for this dependence on activation enthalpy is that at the very high spike temperatures, which are well in excess of the melting point, the diffusion coefficient becomes insensitive to small changes in ΔH_{1v}^m, if ΔH_{1v}^m is small. Thus, the changes in ΔH_{1v}^m which greatly influence the diffusivity at the melting point do not affect the mixing efficiency. If large values of ΔH_{1v}^m are used in the calculation, the diffusion coefficient remains sensitive to small changes in ΔH_{1v}^m, but the mixing efficiency is reduced. In evaluating the discrepancies between the calculated and experimental values of the mixing efficiencies for the different impurity markers, it should be kept in mind that the variations in the mixing efficiencies for the different markers in Cu are small, about a factor of ≈ 2. Approximations in the model are of this magnitude. Agreement between theory and experiment for the different matrices is much better, but there the variations in efficiency between matrices are much larger. We conclude, therefore, that thermal spike model of diffusion based on radiation-enhanced diffusion theory can reasonably account for atomic motion in ion-irradiated metals at low temperatures; the very low vacancy migration enthalpy that is required to obtain agreement with experimental results, however, is not understood in detail.

Finally, we consider the possibility that the cascade region becomes liquidlike during the thermal spike phase of the cascade evolution. Recent results of molecular-dynamics computer simulations of 5-keV cascades in Cu point toward this possibility.[42] Equation (10) can again be applied to calculate IM; however, $D(t)$ now refers to the tracer impurity coefficient in the liquid and not the radiation-enhanced diffusion coefficient. We have performed such calculations for four markers in Cu: Ag, Sb, Au and Sn; the results are listed in Table VI (details of the calculation will be published elsewhere[43]). Impurity diffusion coefficients in liquid Cu were obtained from Ref. 44. The mixing, naturally, is sensitive to the thermal diffusivity of the medium. Using near-neighbor collisional transport to estimate κ ($\kappa = 8\times10^{13}$ Å^2/s), the maximum time for solidification is 0.85 ps, and this maximum occurs for 7.2-keV cascades. For lower energy recoils, the cascades cools at a faster rate, and for higher energies the initial temperature is lower. It can be seen in Table VI that the calculated values for the IM efficiency are lower than experimental values. Applying classical heat-transport theory in a region where extremely-high-temperature gradients exist, however, is questionable. The molecular-dynamics simulations show, for example, that resolidification occurs in 5-keV cascades after 4.3 ps, which corresponds to $\kappa = 1.6\times10^{13}$ Å^2/s. When this value of κ is employed in Eq. (10), rather good results for the magnitude of IM are obtained, although the experiments show greater differences between the IM efficiencies for the different

TABLE V. Calculated values (in Å^5/eV) of the IM efficiency for various tracer impurities in Cu using the radiation-enhanced diffusion model for thermal spike diffusion.

	IM efficiency				
	Ag	In	Nb	Ru	Sb
Experimental	39	47	22	15	43
Normal ΔH_{1v}^m	1.5	4.6	0.1	0.3	4.8
$\frac{2}{3}\Delta H_{1v}^m$	11.9	27.9	2.4	7.5	17.0
$\frac{1}{2}\Delta H_{1v}^m$	27.8	77.4	11.0	37.5	34.3

TABLE VI. Calculated values (in $Å^5/eV$) of the IM efficiency for four tracer impurities in Cu using the liquid-droplet model for thermal spike diffusion. κ refers to the value employed for the thermal diffusivity.

Marker	IM efficiency $\kappa=8\times10^{13}$ $Å^2/s$	$\kappa=1.6\times10^{13}$ $Å^2s$	Expt.
Ag	6.0	30	39
Sb	6.4	32	43
Au	5.6	28	27
Sn	7.4	37	

markers. Liquidlike diffusion in the thermal spike, therefore, may be an important mechanism for thermal spike diffusion in some metals.

VI. CONCLUSIONS

It has been demonstrated here that studies of ion-beam mixing at low temperatures are a powerful method for elucidating fundamental displacement processes in irradiated materials. The present work on metals has shown that atomic mixing in ion-irradiated metals stems predominantly from the collective motion of atoms in a highly excited spike over a very short period of time. Moreover, it was demonstrated that the excited state can be modeled, to a first approximation, within the framework of classical radiation-damage theory involving atomic collisions and radiation-enhanced diffusion. This model provides a natural interpretation for the dependence of the mixing efficiency on such parameters as the cohesive energy of the matrix, the energy density in the cascade, and the diffusivity of the impurity markers in the matrix. In metals which have low melting temperatures and cascades with high-energy densities, liquidlike diffusion during the thermal spike may also be an important mechanism for IM.

The results obtained here for IM apply to other aspects of radiation damage and ion-beam modifications of materials. For example, the efficiency of disordering initially ordered alloys has long been of concern in the field of radiation effects. Our findings here suggest that the disordering process results from a high-temperature diffusion process within the spike. Since ordering energies are much lower than atomic energies in the spike region, diffusion leads to disordering rather than ordering. The disordering that results from the collisional phase of the cascade is of secondary importance. Another outstanding question in radiation-damage research is the mechanism for the formation of vacancy dislocation loops during the evolution of a cascade, i.e., cascade collapse. Our work suggests that the high mobility of vacancies in the spike enables those vacancies created in the collisional phase of the cascade to precipitate out as loops during the lifetime of the excitation. Consistent with this hypothesis is the fact that those metals which have the greatest tendency to form loops are those metals that have high mixing efficiencies, i.e., those with low cohesive energies and spikes with high-energy densities. Finally, we point out that our results can explain why ion-beam-mixed multilayer samples do not form intermetallic compounds and why intermetallic compounds become disordered by low-temperature irradiation. Thermal spike diffusion occurs while the spike is at very hot temperatures, far in excess of the melting temperature, and thus it leads to randomization of atoms. As the spike cools, diffusion is strongly limited and only local rearrangements are possible. Although our understanding of atomic displacement processes are not sufficiently refined to understand these radiation effects in great detail, we believe that our ion-mixing studies do provide a basis for such an understanding.

ACKNOWLEDGMENTS

We are grateful to Mr. P. Baldo, L. J. Thompson, and J. Wallace at Argonne National Laboratory (ANL), and Mr. A. Ghaffari at Caltech for technical assistance. We are also grateful to Dr. B. M. Paine for helpful discussions. One of us (R.S.A.) is grateful to his co-workers, Dr. R. Benedek and Mr. T. Diaz de la Rubia, for use of as-yet-unpublished molecular-dynamics studies, and also their stimulating discussions. This work was supported at Caltech by the U. S. Office of Naval Research under contract No. N00014-84-K-0275 and at ANL and the University of Illinois at Urbana-Champaign by the U. S. Department of Energy Division of Basic Energy Sciences–Materials Sciences under Contracts No. W-31-109-Eng-38 and No. DE-AC02-76ER01198, respectively.

*Present address.

[1]See, e.g., *Ion Implantation and Beam Processing*, edited by J. S. Williams and J. M. Poate (Academic, New York, 1984).

[2]W. L. Johnson, Y. T. Cheng, M. Van Rossum, and M-A. Nicolet, Nucl. Instrum. Methods B **7/8**, 657 (1985).

[3]R. S. Averback, Nucl. Instrum. Methods B **15**, 675 (1986).

[4]H. H. Andersen, Appl. Phys. **18**, 131 (1979).

[5]P. Sigmund and A. Gras-Marti, Nucl. Instrum. Methods **168**, 339 (1980); **182/183**, 25 (1981).

[6]S. Matteson, B. M. Paine, and M-A. Nicolet, Nucl. Instrum. Methods **182/183**, 53 (1981).

[7]W. Moeller and W. Eckstein, Nucl. Instrum. Methods B **7/8**, 645 (1985).

[8]R. S. Averback, R. Benedek, and K. L. Merkle, Phys. Rev. B **18**, 4156 (1978); R. S. Averback, J. Nucl. Mater. **108/109**, 33 (1982).

[9]M. W. Guinan and J. H. Kinney, J. Nucl. Mater. **103/104**, 1319 (1981).

[10]A. J. Barcz, B. M. Paine, and M-A. Nicolet, Appl. Phys. Lett. **44**, 45 (1984).

[11]S.-J. Kim, M-A. Nicolet, R. S. Averback, and P. Baldo, Appl. Phys. Lett. **46**, 154 (1985).

[12]Y. T. Cheng, M. Van Rossum, M-A. Nicolet, and W. L. Johnson, Appl. Phys. Lett. **45**, 185 (1984).

[13]H. Westendorp, Zhong-Lie Wang, and F. W. Saris, Nucl. Instrum. Methods **194**, 453 (1982).
[14]R. S. Averback, D. Peak, and L. J. Thompson, Appl. Phys. A **39**, 59 (1986).
[15]B. Y. Tsaur, S. Matteson, G. Chapman, Z. L. Liau, and M-A. Nicolet, Appl. Phys. Lett. **35**, 825 (1979).
[16]M.-P. Macht and V. Naundorf, J. Appl. Phys. **53**, 7551 (1982).
[17]See, e.g., J. R. Manning, *Diffusion Kinetics for Atoms in Crystals* (Van Nostrand, Princeton, 1968), p. 191.
[18]G. H. Vineyard, Radiat. Effects **29**, 245 (1976).
[19]M. Van Rossum, Y. T. Cheng, W. L. Johnson, and M-A. Nicolet, Appl. Phys. Lett. **46**, 610 (1985).
[20]W. E. King and R. Benedek, J. Nucl. Mater. **117**, 26 (1983).
[21]D. Peak and R. S. Averback, Nucl. Instrum. Methods B **7/8**, 561 (1985).
[22]G. H. Kinchin and R. S. Pease, Rep. Prog. Phys. **18**, 1 (1955).
[23]K. B. Winterbon, *Ion Implantation Range and Energy Deposition Distribution* (Plenum, New York, 1975), Vol. 2.
[24]M. Hansen, and K. Anderko, *Constitution of Binary Alloys* (McGraw-Hill, New York, 1958).
[25]B. M. Paine and R. S. Averback, Nucl. Instrum. Methods B **7/8**, 666 (1985).
[26]J. P. Biersack and L. G. Haggmark, Nucl. Instrum. Methods **174**, 257 (1980).
[27]R. S. Averback and D. Peak, Appl. Phys. A **38**, 139 (1985).
[28]A. Barcz and M-A. Nicolet, Appl. Phys. A **33**, 167 (1984).
[29]J. Westendorp, Ph.D. thesis, FOM Institute for Atomic and Molecular Physics, 1986, p. 87 (unpublished).
[30]A. R. Miedema, Phillips Tech Rev. **36**, 217 (1976).
[31]K. L. Merkle, in *Radiation Damage in Metals*, edited by N. L. Peterson and S. D. Harkness (American Society of Metals, Metals Park, Ohio, 1976), p. 58.
[32]R. S. Averback and M. A. Kirk, in *Surface Alloying by Ion, Electron and Laser Beams*, edited by L. E. Rehn, S. T. Picraux, and H. Wiedersich (American Society of Metals, Metals Park, Ohio, 1986), p. 91.
[33]P. Sigmund, G. P. Scheidler, and G. Roth, Brookhaven National Laboratory Report No. 50083 C-52, 1968, p. 374 (unpublished).
[34]David Lazaraus, Phys. Rev. **93**, 973 (1954).
[35]A. D. Le Clalre, Philos. Mag. **7**, 141 (1962).
[36]See, eg., J. L. Bouquet, G. Brébec, Y. Limoge, in *Physical Metallurgy*, edited by R. W. Cahn and P. Haasen (North-Holland, Amsterdam, 1983), p. 386.
[37]See, e.g., *Vacancies and Interstitials in Metals*, edited by A. Seeger, D. Schumacher, J. Diehl, and W. Schilling, (North-Holland, Amsterdam, 1970).
[38]See, e.g., N.L. Peterson, in *Solid State Physics*, edited by F. Seitz, D. Turnbull, and H. Ehrenreich (Academic, New York, 1968), Vol. 22; J. Nucl. Mater. **69/70**, 3 (1978).
[39]M. W. Finnis (unpublished), quoted by A. D. Brailsford and R. Bullough, in J. Nucl. Mater. **69/70**, 434 (1978).
[40]D. Peak, Proceedings of the 2nd Workshop on Ion Beam Mixing, Pasadena, California, 1985 (unpublished); D. Peak and R. S. Averback (unpublished).
[41]*Metals Reference Book*, edited by C. J. Smithels, 5th ed. (Butterworths, London, 1976).
[42]T. D. Rubia, R. S. Averback, R. Benedek, and W. E. King, Phys. Rev. Lett. **59**, 1930 (1987).
[43]D. Peak and R. S. Averback (unpublished).
[44]A. Bruson and M. Gerl, Phys. Rev. B **19**, 6123 (1979).